II. RADIO ASTRONOMY*

Academic and Research Staff

Prof. A. H. Barrett	Prof. L. B. Lenoir	Dr. S. H. Zisk
Prof. B. F. Burke	Prof. R. P. Rafuse	Patricia P. Crowther
Prof. M. Loewenthal	Prof. D. H. Staelin	E. R. Jensen

Graduate Students

R. J. Allen	E. C. Reifenstein III	K. D. Thompspn
N. E. Gaut	A. E. E. Rogers	A. Vander Vorst
J. M. Moran, Jr.	D. H. Steinbrecker	Z. Vugrinec
G. D. Papadopolous		T. L. Wilson

A. TEMPERATURE DEPENDENCE OF THE MICROWAVE EMISSIVITY OF NaCl SOLUTIONS

Satellite-borne microwave sensors designed to probe the atmosphere will have sea water as a background over two-thirds of the earth's surface. It is therefore important to know its microwave properties.

The emissivity of sea water depends upon a number of factors, notably wavelength, temperature, viewing angle, and salinity. Based on measurements of the complex dielectric constant of NaCl solutions by Collie, Hasted, and Ritson[1,2] the temperature

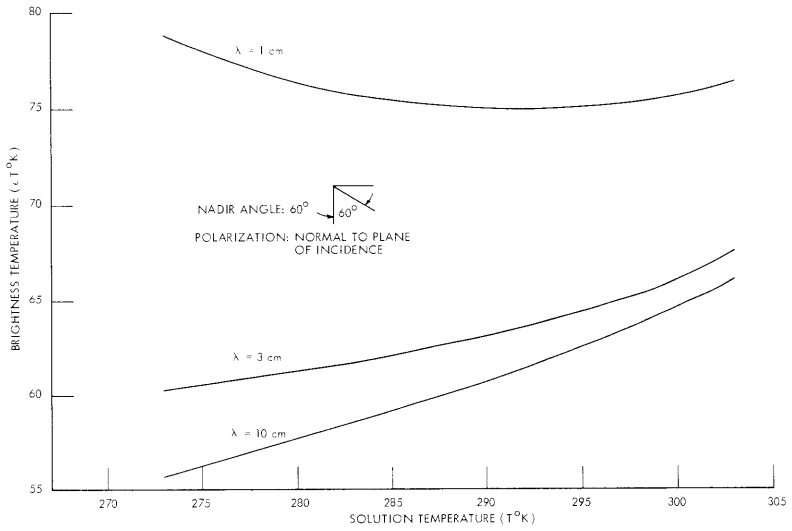

Fig. II-1. Microwave brightness temperature of salt water (0.66 m/l) as a function of thermometric temperature, viewed 60° from the surface normal with the observed $\vec{E}$ parallel to the surface.

*This work was supported principally by the National Aeronautics and Space Administration (Grant NsG-419 and Contract NSR-22-009-120); and in part by Lincoln Laboratory Purchase Order No. 748.

dependence of a 0.66 m/l NaCl solution has been calculated. A sample is shown in Fig. II-1 for 1-, 3-, and 10-cm wavelengths, with a viewing angle of 60°, and polarization normal to the plane of incidence. The important feature at smaller wavelengths is the partial compensation of increasing thermometric temperature by decreasing emissivity. This result will be helpful in reducing the uncertainty of determining the sea surface brightness temperature at these wavelengths.

N. E. Gaut

References

1. C. H. Collie, J. B. Hasted, and D. M. Ritson, Proc. Phys. Soc. (London) 60, 145-160 (1948).
2. J. B. Hasted, D. M. Ritson, and C. H. Collie, J. Chem. Phys. 16, 1 (1948).

B. MICROWAVE ABSORPTION MEASUREMENTS OF THE TERRESTRIAL ATMOSPHERE

Observations of sunlight extinction by the atmosphere at five frequencies around the 1.35-cm water-vapor spectral line are now in progress. The present data are being collected to provide information during winter meteorological conditions to supplement

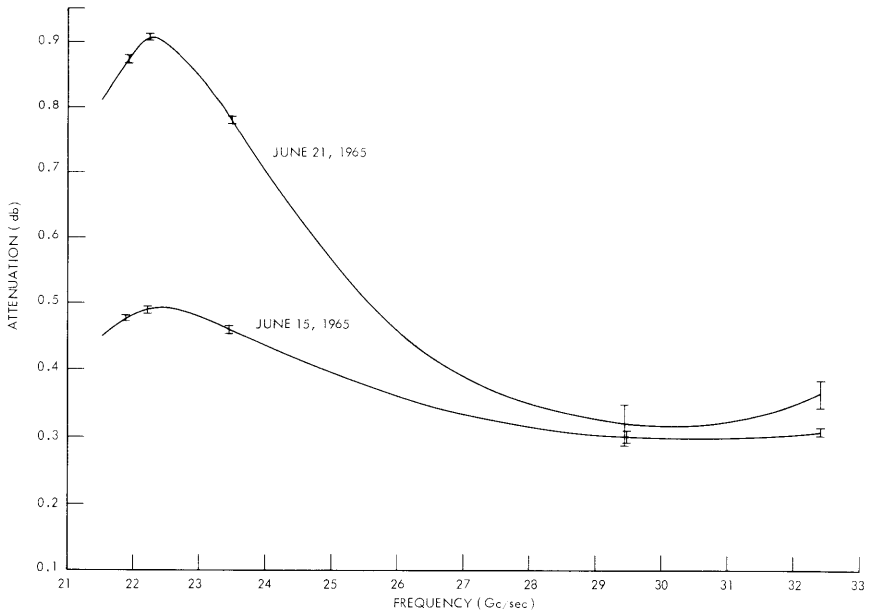

Fig. II-2. Zenith atmospheric attenuation near the water-vapor resonance at 22.235 Gc/sec (1.35-cm wavelength observed on two days with quite different water-vapor distributions.

the data taken last summer. The ultimate goal of the program is to develop inversion techniques that will relate the microwave extinction spectrum to the total water vapor and its vertical distribution.

Thus far, 36 sunsets have been monitored from the 28-ft radio telescope at Lincoln Laboratory, M.I.T. Thirty-three of these observations have accompanying radiosonde information. The radiosondes have been launched either at the Reservoir Hill Launch Facility at Hanscom Field, or at M.I.T in Cambridge, for the most part within the periods of the sun observations.

Figure II-2 shows two extremes for the water-vapor spectral line obtained on the dates noted.

N. E. Gaut, D. H. Staelin

C. MEASUREMENTS OF CONTINUUM RADIATION FROM COSMIC RADIO SOURCES AT THE HAYSTACK RESEARCH FACILITY

The Haystack Research Facility has been described by H. G. Weiss, in Lincoln Laboratory Technical Report 365. A cursory description of the radiometric system was given in Quarterly Progress Report No. 78 (pages 27-35).

1. Absolute Flux Measurements

The antenna temperature $T_M(\theta', \phi')$ measured with an antenna of effective aperture $A(\theta-\theta', \phi-\phi')$, directed toward θ', ϕ', is expressed by

$$T_M(\theta', \phi') = \frac{1}{\lambda^2} \int_{4\pi} A(\theta-\theta', \phi-\phi')\, T(\theta, \phi)\, d\Omega, \tag{1}$$

where λ is the wavelength of observation, and $T(\theta, \phi)$ expresses the brightness of the surroundings in direction θ, ϕ. If there is a source of radio emission contained within the solid angle Ω_S, one may write

$$T(\theta, \phi) = T_B(\theta, \phi) + T_S(\theta, \phi),$$

where $T_B(\theta, \phi)$ contains the "background" radiation, from the atmosphere, the ground, and so forth, and $T_S(\theta, \phi)$ represents the source. T_B extends over 4π steradians, while T_S is presumed to be zero outside of Ω_S. Rearranging (1), we have

$$T_A(\theta', \phi') = T_M(\theta', \phi') - \frac{1}{\lambda^2} \int_{4\pi} A(\theta-\theta', \phi-\phi')\, T_B(\theta, \phi)\, d\Omega$$

$$= \frac{1}{\lambda^2} \int_{\text{source } \Omega_S} T_S(\theta, \phi)\, A(\theta-\theta', \phi-\phi')\, d\Omega. \tag{2}$$

Fig. II-3. Radiometer instrument box connected to the cornucopia horn antenna.

$T_A(\theta', \phi')$ is the measured antenna temperature after base-line subtraction. It is usual to express $A(\Omega) = \eta A_g f(\Omega)$, where η is the antenna efficiency, A_g is the geometric area of the aperture, $f(\Omega)$ is the antenna polar diagram, and $f(0) = 1$.

If the source distribution is contained within a solid angle much smaller than the antenna half-power beamwidth and the antenna is pointed directly at the source, then (2) evidently reduces to

$$T_A = \frac{1}{\lambda^2} \eta A_g \int_{\Omega_S} T_B(\Omega)\, d\Omega. \tag{3}$$

The total flux of a cosmic radio source received at the Earth's surface is given by

$$S\nu = \frac{2k}{\lambda^2} \int_{\Omega_S} T_B(\Omega)\, d\Omega; \tag{4}$$

consequently,

$$S\nu = \frac{2kT_A}{\eta A_g}. \tag{5}$$

A standard cornucopia horn antenna,[1] manufactured by Bell Telephone Laboratories, Inc., was procured for flux measurements at the Haystack facility. The effective aperture area ηA_g has been measured on the antenna test range at Lincoln Laboratory, and the results agree well with the theoretical calculations.[2] The horn antenna is mounted as a transit instrument (movable in elevation along the local meridian) and may be directly connected to the radiometric instrument box when it is removed from the 120-ft antenna. Figure II-3 shows the installation. This antenna was used for transit drift-scan observations of the strong radio sources in Cassiopeia and Taurus at 8.25 GHz during January 1966. Data from a single drift scan were recorded on punched paper tape, along with appropriate noise-tube calibrations, and subsequently were analyzed by

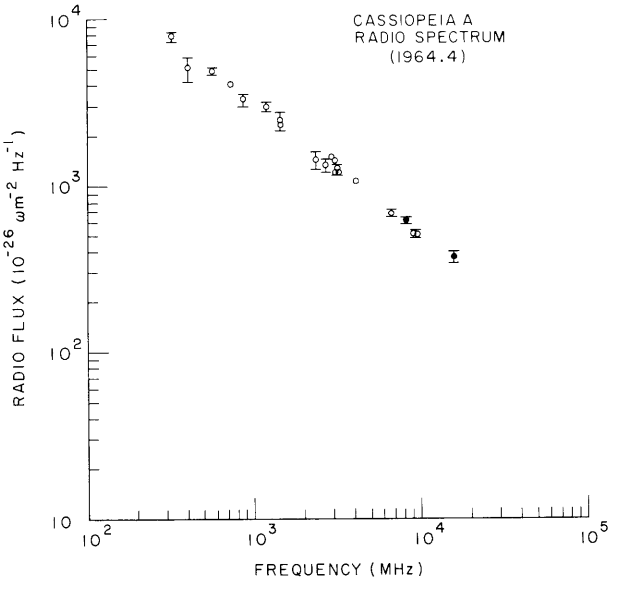

Fig. II-4. The radio spectrum of the strong source in Cassiopeia. O = other measurements. ● = present measurements.

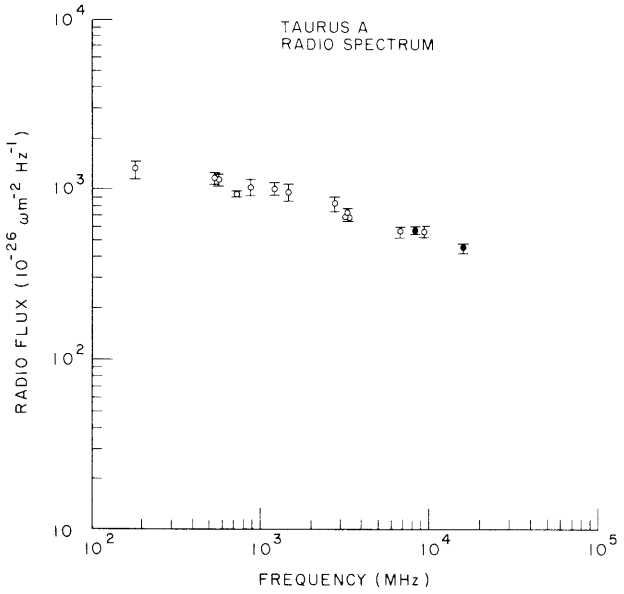

Fig. II-5. The radio spectrum of the strong source in Taurus. ○ = other measurements. ● = present measurements.

computers. Drift scans were taken at slightly different elevations on successive evenings, and the final antenna temperature was determined from the peak point of all observations. This was corrected for atmospheric extinction, equipment losses, and nonlinearity, and converted to a flux value by using Eq. 5. A complete description of the observational technique, the method of data reduction, and the measurement of the equipment effects will be given in a future progress report, together with the final numerical results. The result for the observations of Cas A is compared with the measurements of other observers in Fig. II-4. The antenna temperature measured on Taurus must also be corrected for the linear polarization of the radiation. This quantity was measured with the 120-ft antenna by using a technique that is described below. The results for Taurus are compared with other work in Fig. II-5.

2. Observations with the 120-ft Paraboloid

In order to correctly interpret measurements of antenna temperature with the 120-ft antenna, it is, of course, necessary to know the characteristics of the antenna. The instrumental effects of radio-astronomical interest are the antenna efficiency and the instrumental polarization, and possible elevation dependences of these quantities.

a. Antenna Efficiency

When the cosmic radio source has an angular size of the same order of magnitude as the angular size of the antenna beam, Eq. 5 is not valid. One of two things may be done: The source may be modelled and a correction factor to the antenna temperature T_A may then be calculated or a contour map of $T_A(\theta', \phi')$ may be integrated. The former technique proceeds as follows: from Eq. 2, when the antenna is pointing directly at the source,

$$T_A = \frac{A_g}{\lambda^2} \int_{\Omega_S} f(\Omega)\, T_S(\Omega)\, d\Omega.$$

One then models the source: $T_S(\Omega) = T_o g(\Omega)$, where $g(\Omega)$ is some function such that $g(0) = 1$. Hence, from Eq. 4,

$$S_\nu = \frac{2kT_o}{\lambda^2} \int_{\Omega_S} g(\Omega)\, d\Omega.$$

But,

$$2kT_A = \frac{\eta A_g}{\lambda^2} 2kT_o \int_{\Omega_S} f(\Omega)\, g(\Omega)\, d\Omega.$$

Consequently,

$$\eta = \frac{2kT_A}{S_\nu A_g} \frac{\int_{\Omega_S} g(\Omega)\, d\Omega}{\int_{\Omega_S} f(\Omega)\, g(\Omega)\, d\Omega}. \tag{6}$$

For future reference, we define

$$S = \int_{\Omega_S} g(\Omega)\, d\Omega$$

and

$$M = \int_{\Omega_S} f(\Omega)\, g(\Omega)\, d\Omega.$$

If the antenna pattern is known, then η is defined when the source model is specified.

On the other hand, the second method, or integration technique, proceeds as follows: From Eq. 2, if $T_A(\theta', \phi')$ is known over some region $\Omega_m > \Omega_S$, then upon integrating $T_A(\theta', \phi')$ over this region, we have

$$\int_{\Omega_m} T_A(\Omega')\, d\Omega' = \frac{1}{\lambda^2} \int_{\Omega_m} \int_{\Omega_S} A(\Omega - \Omega')\, T_B(\Omega)\, d\Omega d\Omega'. \tag{7}$$

But

$$\int_{\Omega_m} A(\Omega)\, d\Omega = \eta A_g \int_{\Omega_m} f(\Omega)\, d\Omega.$$

Let us define $\Omega_B = \int_{\Omega_m} f(\Omega)\, d\Omega$. Equation 7 then reduces to

$$2k \int_{\Omega_m} T_A(\Omega')\, d\Omega' = \frac{2k}{\lambda^2} \int_{\Omega_S} T_B(\Omega)\, d\Omega\, \eta A_g \Omega_B = S_\nu \eta A_g \Omega_B;$$

consequently,

$$\eta = \frac{2k \int_{\Omega_S} T_A(\Omega')\, d\Omega'}{S_\nu A_g \Omega_B} . \tag{8}$$

The advantages of the second technique are that it is independent of models of the radio source, and only the integral over part of the antenna polar diagram is required.

The first technique has been applied to calculate the antenna efficiency of the 120-ft paraboloid by using the values of radio flux measured with the cornucopia horn at 8.25 GHz.

Results from Cas A

The following model is suggested by high-resolution interferometer studies[3]: A ring of emission of diameter W = 4.0 ft and thickness d ≪ W. The antenna beam is modelled as a circularly symmetric Gaussian with full width at half-power of 4.2 ft. The last assumption is supported by observations of the weak point source 3C273. These assumptions yield S/M = 1.82, and antenna efficiency $\eta = 0.31 \pm 0.02$ at 40° elevation.

Results from Tau A

The Taurus model[4] is a two-dimensional Gaussian, 4.2 ft × 2.6 ft; the flux is polarized 8% at 147° as will be described subsequently. This yields S/M = 1.63, and antenna efficiency $\eta = 0.29 \pm 0.02$ at 40° elevation.

The close agreement is probably deceptive; the results are very dependent on the source model parameters. Besides the fact that few observers agree on a satisfactory model, it is known that the structure of a source generally depends somewhat on frequency, so that models based on low-frequency observations are hazardous. Plans have been made to apply the second method for a more reliable estimation of η.

Measurements of 2% precision have been made of the elevation dependence of the antenna efficiency. Results of observations of peak antenna temperature made on a number of strong sources are compiled in Fig. II-6. No azimuth dependence of the antenna efficiency >0.01% has been noticed. The measurements on each source are corrected for atmospheric extinction and normalized to 40° elevation. The ordinate of Fig. II-6 may be identified with the antenna efficiency relative to 40° elevation. The general shape of the curve is understandable as sag of the subreflector at the prime focus, and a slight movement of the instrument box as the antenna is raised in elevation, both effects tending to alter the focal length of the antenna.

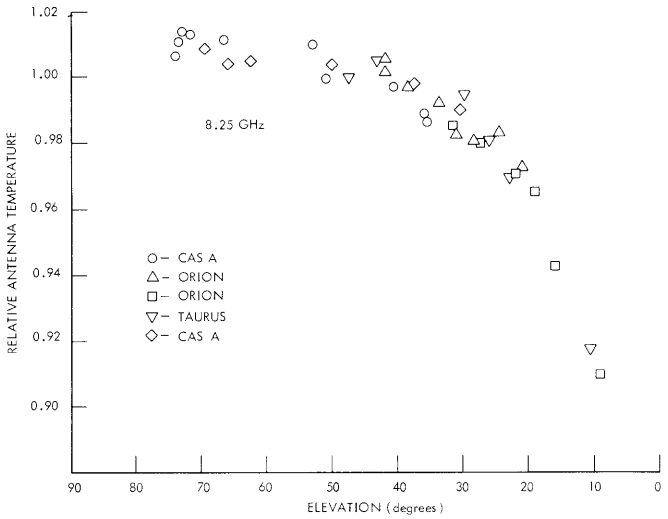

Fig. II-6. Relative antenna temperature versus elevation for a number of sources normalized to 1 at 40° elevation.

b. Instrumental Polarization

Measurements of the linear polarization of the radiation from cosmic sources is usually made by rotating a linearly polarized feed horn of the antenna, and determining the constants in the equation

$$T(A) = T_A(1 + p\cos 2(A-\phi)), \tag{9}$$

where

T_A = average antenna temperature

p = fractional linear polarization of the source

A = parallactic angle of feed (position angle of E on the celestial sphere)

ϕ = parallactic position angle of the polarized component of the radiation from the source.

Unfortunately, such measurements are usually contaminated by two effects: baseline shift caused by rotating antenna sidelobes picking up the partially polarized radiation from the earth, and an apparent dependence of the antenna efficiency with feed angle. The first problem can be overcome by suitable choice of observing techniques; the second can be measured by observations on a cosmic source of unpolarized radio emission. After many attempts, we conclude that the following observing technique allows unambiguous separation of these two effects; it consists essentially of always using the 120-ft antenna as if it were polar mounted. Although such a technique is hardly new in

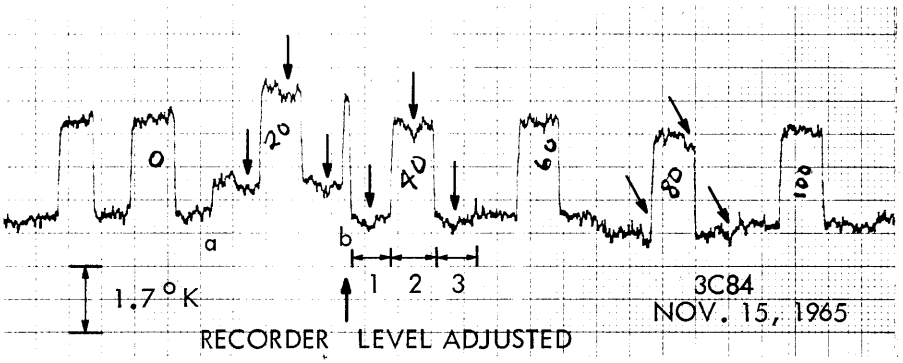

Fig. II-7. Example of the effects of varying radome space frame aperture blockage on the measurements of a weak source.

radio astronomy, it seems especially useful for antennas in radomes. Data taken when the antenna is tracking a source is corrected by subtracting data taken while the antenna is tracking the sky over exactly the same place on the radome. The usefulness of the technique is quite clear from Fig. II-7. In region 1, the sky is tracked at the sidereal rate a few half-power beamwidths ahead of the source. One then waits until the position of the earth brings the source into the same place on the radome, and then the source is tracked. In region 3, a measurement (again over exactly the same range of azimuth and elevation) is taken after the source has moved away. All three observations are made at the same feed angle, designated "40" on the chart. The arrows indicate features about 4 times the r.m.s. noise that seems to appear at the same azimuth and elevation each time, thereby suggesting a varying amount of aperture blockage attributable to the radome struts. Figure II-7 also shows the base-line change as the feed is rotated. As point a, the feed was rotated from "0" (0°) to "20" (36°). Note the change in base line. At b, the rotation from "20" to "40" (72°) would have put the observation off the chart, and the recorder level was readjusted.

The apparent dependence of antenna efficiency with feed angle was investigated by making observations of the type just described as a series of different feed angles on the strong unpolarized sources Cas A and Orion A: A compendium of data indicates that the parameters of Eq. 9 (where A is now the feed angle in "az-el" coordinates) are $100p = 1.05 \pm 0.2$, $\phi = 146 \pm 3°$ measured eastward from north on the celestrial sphere. There is some indication of a very small variation of these quantities with elevation and, perhaps, azimuth, the origin of which is not yet fully understood. Further observations are planned.

c. Observations of Other Cosmic Sources

Now that we are beginning to understand the instrumental effects, the original task of observing the flux and polarization properties of radio sources is being taken

up again. The strong radio source in Taurus and a weak source in Perseus were the first candidates, and the results at 8.25 GHz are tabulated in Table II-1. Angular size

Table II-1. Results of observations.

	Peak Antenna Temperature	Polarization (%)	Position Angle	Angular Size (α)	δ	Radio Flux
Taurus A (3C144)	37.65 ± 0.03 °K	8.0 ± 0.4	147 ± 4°	2.8'	2.5'	567 ± 50
Perseus A (3C84)	2.51 ± 0.01 °K	<0.3	—	<30"	1.3'	18 ± 3

is measured in minutes of arc. The units of radio flux are 10^{-26} watt m^{-2} Hz^{-1}.

The results for Taurus are in good agreement with the work of other observers, especially the observations of Gardner[5] at 6 cm, using an antenna having nearly the same half-power beamwidth as the Haystack antenna.

The radio source Perseus A has been identified with the peculiar galaxy[6] NGC 1275, and is observed to have a curious spectrum of positive spectral index[7] above 3 GHz. The present measurement confirms this, and we may add, first, that the radiation is essentially unpolarized, second, the source is less than 30 seconds of arc in right ascension and has a width of approximately 1.3' in declination. The last results have not been reported before, and are important to the models of the physical processes responsible for the radiation.

R. J. Allen, A. H. Barrett

References

1. R. W. Friis and A. S. May, AIEEE Trans. Part 1, Vol. 77, p. 97, 1958.
2. A. Sotiropoules and J. Ruze, "Haystack Calibration Antenna," Technical Report 367, Lincoln Laboratory, M.I.T., December 1964.
3. M. Ryle, B. Elsmore, and A. Neville, Nature 205, 1259 (1965).
4. J. W. Baars, P. G. Mezger, and H. Wendker, Astrophys. J. 142, 122 (1965).
5. F. F. Gardner, Australian J. Phys. 18, 385 (1965).
6. W. A. Dent and F. T. Haddock, Quasi-Stellar Sources and Gravitational Collapse (University of Chicago Press, Chicago, Ill., 1965), chapter 29.
7. W. A. Dent and F. T. Haddock, Nature 205, 487 (1965).

D. OBSERVATIONS OF THE MOON

Radiometric observations[1] of the moon were made during the summer of 1964 with the 28-ft paraboloid antenna at Lincoln Laboratory. The first series of observations

was conducted between June 15th and August 15th, 1964, using a five-channel Dicke radiometer.[2] The channels were centered at 32.4, 29.5, 25.5, 23.5, and 21.9 GHz. A total of 340 drift scans of the moon was taken on 15 different days. Typical shift scans through the center of the moon are shown in Fig. II-8.

Because of the moon's rotation, the temperature of every point on its surface can be expressed as a Fourier series with a fundamental period of 29.53 days. The brightness temperature is usually modelled as

$$T_B(\theta, \ell, f, t) = T_{B_o} + \cos^{1/4} \ell \sum_n T_{B_n}(f) \cos (n\omega t - n\theta - \psi_n(f)),$$

where θ and ℓ are the selenographic longitude and latitude, and f is the frequency of observation. The quantity measured by the antenna is the antenna temperature, which is the convolution of the antenna pattern with the source brightness temperature. The antenna smoothing was not severe, since the half-power beamwidth is 5.0 minutes of arc at 32.4 GHz, while the diameter of the moon is approximately 30 minutes of arc.

The Fourier components T_{B_n} and ψ_n were deduced from the shapes of the drift scans taken through the center of the moon over two lunar periods. This method is more

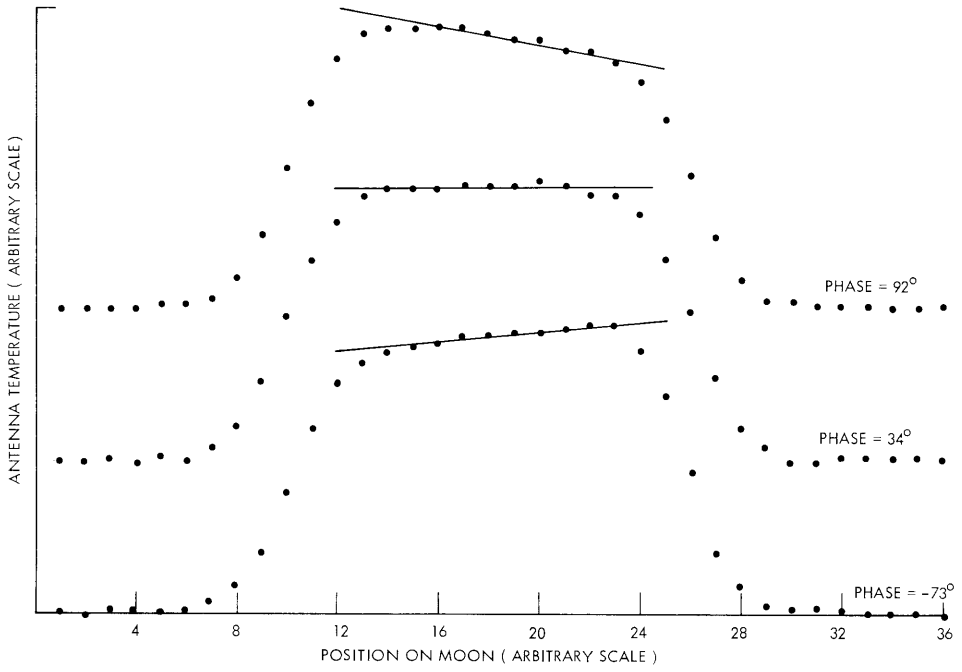

Fig. II-8. Average of three drift scans taken on three different days. Phase angle is measured from full moon. Amplitudes have been scaled to give center temperature of 217°K.

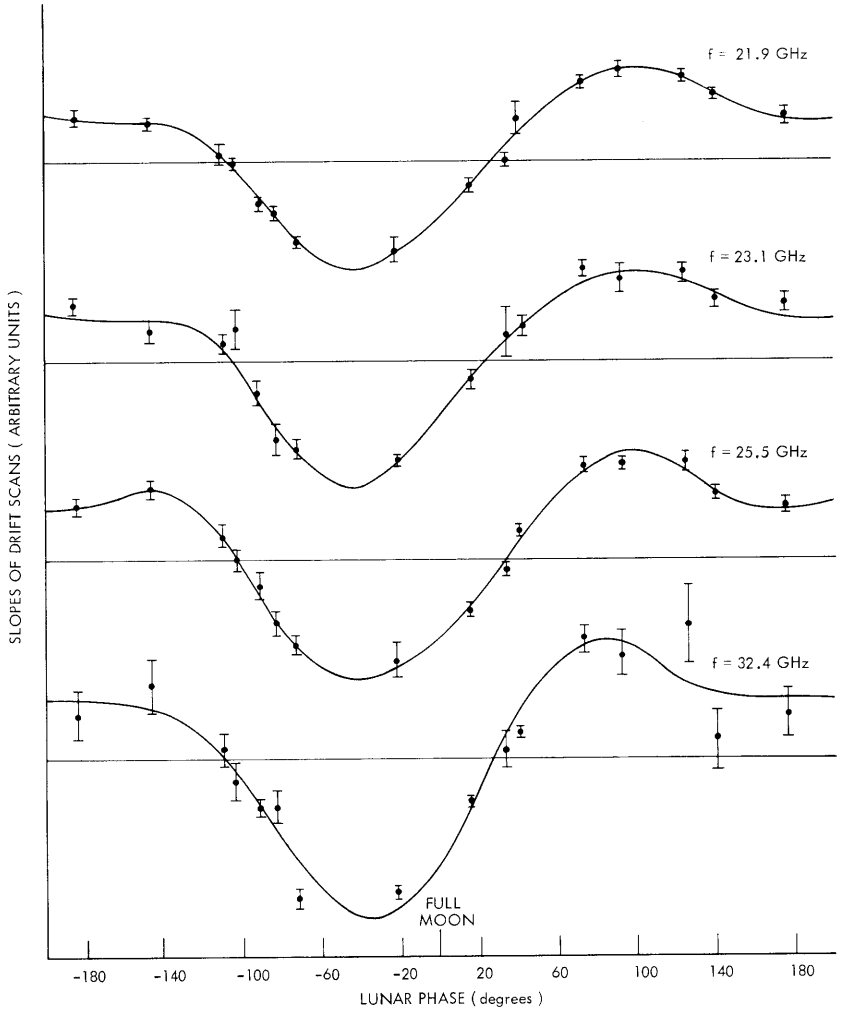

Fig. II-9. Slopes of central region of drift scans vs phase. Curves are two harmonic Fourier series. Notice that the second harmonic of the slope, which is proportional to the second harmonic of the brightness temperature, is necessary for a good fit of the data.

accurate than the customary technique of analyzing the magnitudes of the drift scans. The center temperatures of all scans were normalized to 217°K and the 9 central data points of each were fitted with a straight line using a minimum-square-error criterion as shown in Fig. II-8. Figure II-9 shows the slopes for 4 of the channels as functions of the lunar phase. These slope functions were Fourier analyzed. The Fourier coefficients obtained are proportional to the Fourier coefficients of the brightness distribution. The values obtained for T_{B_1}, T_{B_2}, ψ_1, and ψ_2 are listed in Table II-2. These values are essentially independent of the lunar model used. This is the lowest frequency at which the second harmonic has been measured.

The first-harmonic amplitude yields the value

$$\sqrt{\frac{ps}{K}}\,\frac{\epsilon}{\sigma^2} = 6900$$

at 32.4 GHz. Here, p, s, and K are the density, specific heat, and thermal conductivity in cgs units, ϵ is the dielectric constant and σ is the conductivity in mhos per meter.

Table II-2. Measured values of Fourier coefficients of the Moon's brightness temperature.

Frequency (GHz)	T_{B_o} (°K) (assumed)	T_{B_1} (°K)	ψ_1 (°)	T_{B_2} (°K)	ψ_2 (°)	T_{B_3} (°K)
21.9	217	21 ± 2	41 ± 5	5 ± 1	38 ± 5	<1
23.5	217	22	48	6	31	<1
25.5	217	25	42	6	40	<1
32.4	217	29	41	8	38	<1

This assumes a homogeneous surface with parameters independent of temperature. The thermal inertia, $(Kps)^{1/2}$, has been found from lunar infrared observations to be 0.001 (CGS) which is characteristic of material having very low density and thermal conductivity. Taking p = .2 grams/cm^3, K = 2.5×10^{-6} cal sec^{-1} cm^{-1} °K^{-1}, s = .2, and ϵ = 1.5 it follows that σ = .05 mhoes/meter. This is consistent with very dry sand. The second harmonic data does not give a clear distinction between the homogeneous and stratified surface models.

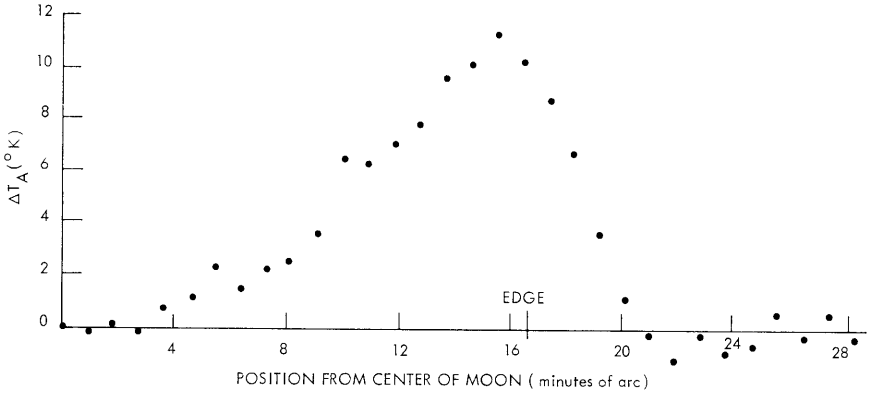

Fig. II-10. Horizontal minus vertical polarization antenna temperature obtained August 4, 1964. Central temperatures have been scaled to 217°K.

The other set of observations was conducted at 35 GHz using the Lincoln Laboratory radiometer on the same 28-foot antenna. Drift scans were taken through the center of the moon near transit with polarization alternately parallel and perpendicular to the plane of incidence on successive scans. The antenna temperatures recorded with orthogonal polarizations differ because the emissivity of the surface depends on the polarization of the radiation as well as the angle of incidence. Figure II-10 shows the average difference between three pairs of scans.

Models for the lunar surface were generated on the computer by assuming that it

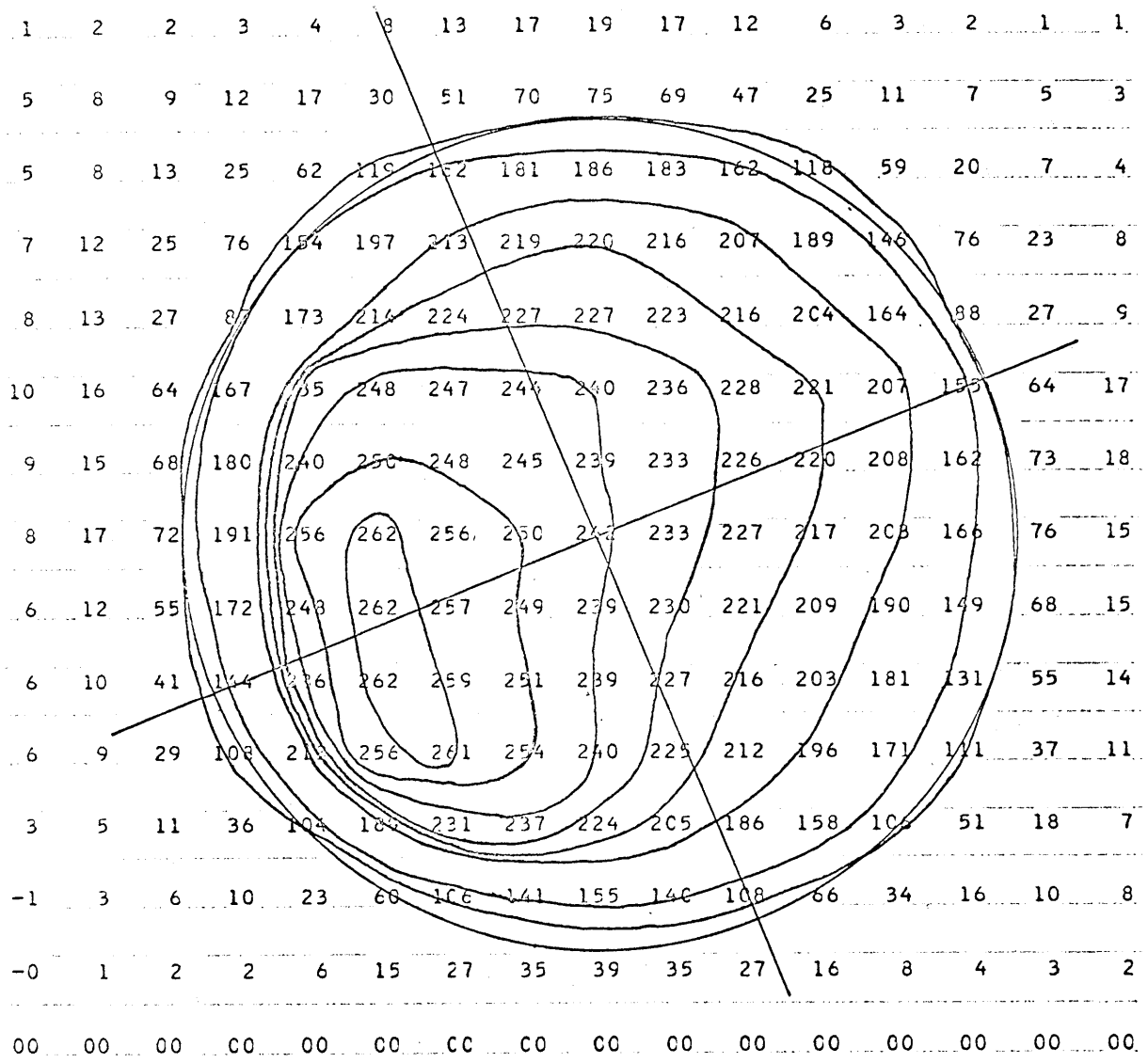

Fig. II-11. Antenna temperature distribution obtained on November 27, 1964. Grid spacing, 2.69 minutes of arc; lunar phase, 100°; frequency, 35.0 GHz; antenna beamwidth, 4.4 minutes of arc.

consists of randomly oriented smooth facets whose normals are gaussianly distributed about the local normal. The expectation of the Fresnel reflection coefficients for each point on the moon were computed. If σ is the angular deviation of the facets and ϵ is the dielectric constant, then the data in Fig. II-10 are consistent with the following parameters:

σ	ϵ
0°	1.5 ± .1
15°	1.7
30°	2.3

These results do not conflict with the value of 2.8 for the dielectric constant obtained from the radar experiments at 68-cm wavelength since the radar reflection may come largely from the denser substratum.

Many drift scans were taken over the entire lunar disk with both radiometer systems in order to map the temperature distribution at various phases. Figure II-11 shows a map made from 10 scans at 35.0 Kmc/s spaced at 3 minutes of arc intervals. It was made eight days after full moon while the left half of the disk was still sunlit.

We are indebted to Mr. J. Freedman and Dr. J. Cogdell for making available the facilities at Lincoln Laboratory.

J. M. Moran, A. H. Barrett, D. H. Staelin

References

1. J. M. Moran, "Radiometric Observations of the Moon near One-Centimeter Wavelength," S.M. Thesis, Department of Electrical Engineering, M.I.T., 1965.
2. D. H. Staelin, "Microwave Spectrum of Venus," Sc.D. Thesis, Department of Electrical Engineering, M.I.T., 1965.